Nuclear Targeting Dynamics of Gold Nanoclusters for Enhanced Therapy of HER2$^+$ Breast Cancer

Yuling Wang,[†] Jiji Chen,[†] and Joseph Irudayaraj*

Bindley Bioscience Center, Birck Nanotechnology Center, Department of Agricultural and Biological Engineering, 225 South University Street, Purdue University, West Lafayette, Indiana 47907, United States. [†]These authors contributed equally to this work.

ABSTRACT

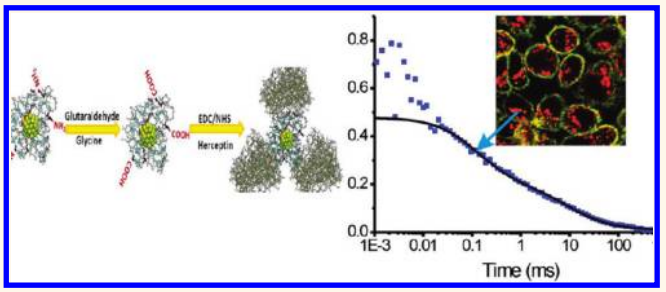

Recent advances in fluorescent metal nanoclusters have spurred tremendous interest in nanomedicine due to the ease of fabrication, excellent biocompatibility, and, more importantly, excellent wavelength-dependent tunability. Herein, we report our findings on fluorescent BSA-protected gold nanoclusters (AuNCs), ~2 nm in size conjugated with Herceptin (AuNCs-Her), for specific targeting and nuclear localization in ErbB2 over-expressing breast cancer cells and tumor tissue as a novel fluorescent agent for simultaneous imaging and cancer therapy. More interestingly, we found that AuNCs-Her could escape the endolysosomal pathway and enter the nucleus of cancer cells to enhance the therapeutic efficacy of Herceptin. We elucidate the diffusion characteristics (diffusion time and number of diffusers) and concentration of the fluorescing clusters in the nucleus of live cells. Our findings also suggest that the nuclear localization effect of AuNCs-Her enhances the anticancer therapeutic efficacy of Herceptin as evidenced by the induction of DNA damage. This study not only discusses a new nanomaterial platform for nuclear delivery of drugs but also provides important insights on nuclear targeting for enhanced therapy.

KEYWORDS: gold nanoclusters · nuclear nanomedicine · single particle characterization · DNA damage · HER2$^+$ targeting

Nanomedicine has made significant advances because of the infusion of sophisticated nanostructures in diagnostics and therapeutics. Understanding the dynamics of nanomaterials in cells, especially the nucleus, critical for nuclear targeting and therapy remains largely an underexplored field. Different types of nanomaterials such as gold, silver, silica, magnetic nanoparticles,[1−4] polymer and liposome nanoparticles,[5−8] and quantum dots (QDs)[9,10] have been developed to target live cells for drug or gene delivery for theranostics. Most of the past studies have demonstrated the potential of these nanomaterials in cancer treatment but primarily in cancer cell targeting or uptake studies and drug delivery. A thorough understanding of the intracellular fate in relation to the nucleus and the efficacy of nuclear drug delivery has not been explored. Nanoparticles of very small size have been postulated to enter the nucleus through the nuclear pore complex, which is about 6−10 nm in diameter and acts as the gateway for nucleo-cytoplasmic exchange.[11] Uptake of nanoparticles beyond this size can be triggered with the aid of a nuclear localization signal (NLS).[12] Gold nanoparticles functionalized with an arginine-glycine-aspartic (RGD) peptide and NLS peptide have been used for cancer cell nuclear targeting.[13] Most of the past studies focus on receptor targeting while few on nuclear targeting because of the challenges in the nuclear delivery of nanoparticles. The nucleus of eukaryotic cells contains a majority of the genetic materials in which DNA replication and transcription occur. Hence strategies for intracellular quantification of nuclear materials will enhance our understanding of nuclear delivery and targeting therapeutics.

Fluorescent nanoparticles, such as QDs, have been widely used for intracellular imaging due to their intense fluorescence. However, the toxicity of QDs limits its use in nanomedicine.[14] Gold nanoclusters (AuNCs) of ~2 nm in size are attractive because of their strong fluorescence emission which permits quantification of nucleus targeting materials at single particle sensitivity. To examine these particles, a single wavelength source is sufficient for simultaneous excitation of nanoclusters of varying emission, similar to QDs.[15−17] Fluorescent AuNCs are also biocompatibile and photostable

* Address correspondence to josephi@purdue.edu.

Received for review August 21, 2011 and accepted November 6, 2011.

Published online November 07, 2011
10.1021/nn2032177

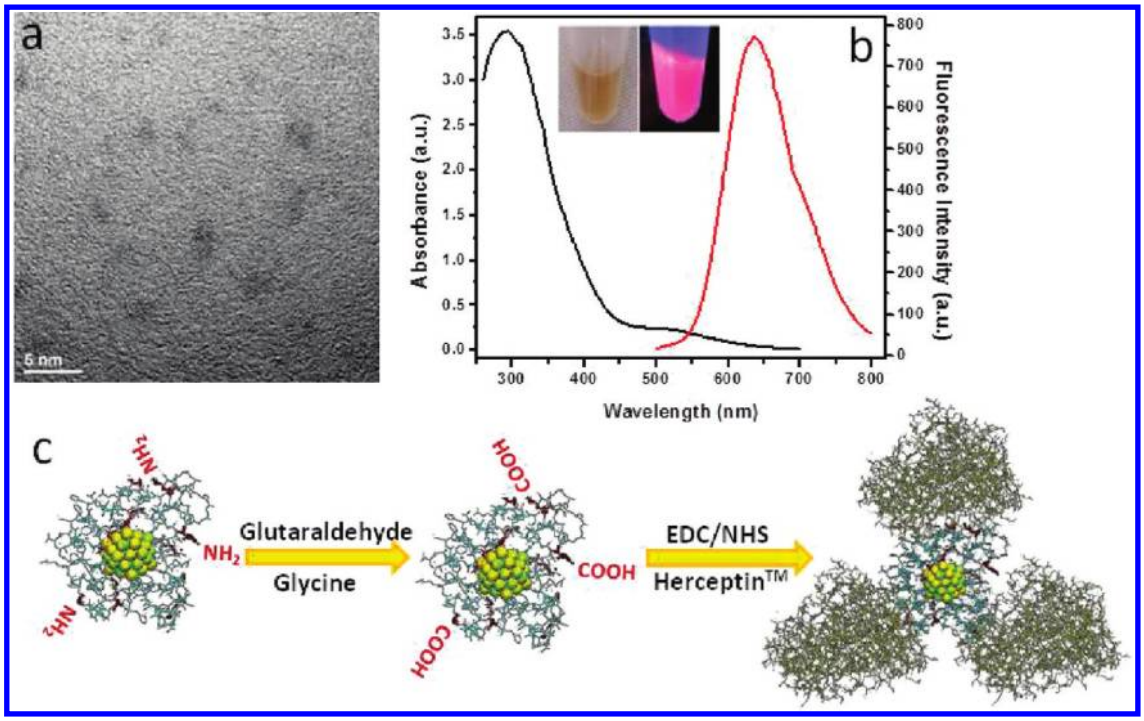

Figure 1. (a) TEM image of the as-prepared AuNCs; (b) UV−vis absorbance and fluorescent spectrum of AuNCs, and (c) schematic of AuNCs-Her conjugation.

and can serve as excellent bioimaging contrast agents for nuclear nanomedicine, which has only been sparsely addressed.[18−20]

Trastuzumab (Herceptin), a humanized monoclonal antibody targeting the extracellular domain of ErbB-2 receptor, is over-expressed in 25−30% of breast cancers and distant metastases.[21] However, the response rate to Herceptin has only been 7−35% in clinical patients.[22] A limiting factor in treatment efficacy enhancement is the lack of an effective drug delivery vehicle to assist in the translocation of the drug from the cytoplasm to the nucleus.[23,24] The therapeutic mechanism of Herceptin as reported reveals that cell proliferation decreases due to an increase in the frequency of DNA double strand breaks in the nucleus.[25] However, more recently, studies point to the fact that nuclear localization sequence (NLS)-conjugated trastuzumab (Herceptin) could kill breast cancer cells that are resistant to trastuzumab by inducing DNA damage, affirming the importance of developing nuclear delivery strategies for effective therapy.[26]

Herein, we hypothesize that Herceptin-conjugated AuNCs, that is, AuNCs-Herceptin (AuNCs-Her), could facilitate effective passage of Herceptin through the nuclear pore and into the nucleus to significantly enhance the anticancer effect of the drug. Therefore, fluorescent correlation spectroscopy (FCS) and fluorescence lifetime imaging (FLIM) were used in this study to track the dynamics of nanoprobes at single particle sensitivity. FCS is a noninvasive single particle fluorescence technique based on autocorrelation of temporal behavior of fluorescence fluctuation. FCS analysis provides information on the diffusion time, absolute concentration of the diffusers, and binding kinetics and opens a new direction for tracking the biochemical pathway in intact cells and organs.[27] FLIM could separate the species based on differences in the exponential decay rate of fluorescence (lifetime),which is independent of the local concentration of fluorescence molecules and the excitation intensity.[28] In this study, we combine FCS with FLIM to report on the diffusion of AuNCs-Her and its entry into the nucleus in live cell conditions. An effective mode of cancer therapy could constitute the specific delivery of high levels of therapeutic agents to hypersensitive subcellular sites such as the nucleus of tumor cells without affecting healthy cells and tissues.[29] Photothermal therapy with cell surface targeting is an effective method for cancer therapy.[30] However, this method is limited by penetration depth of the laser (*e.g.*, <400 μm for a two-photon excitation[31]). In addition, only a few cells can be illuminated at a time in a given focal volume.

RESULTS AND DISCUSSION

Characterization of AuNCs and Bioconjugated AuNCs-Her. Biocompatible fluorescent AuNCs, ~2 nm in size (Figure 1a), were prepared according to the method proposed by Xie *et al.*[16] Its absorption and emission spectra (Figure 1b) show that its characteristic surface plasmon peak disappears and a strong bright near-infrared peak emerges at 640 nm. The strong fluorescence of AuNCs was due to the d-band excitation as reported.[32] Figure 1c shows the scheme for the

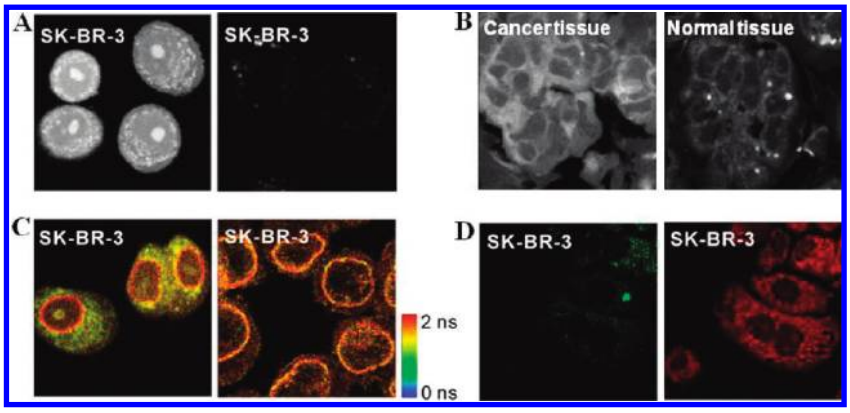

Figure 2. (A) Confocal fluorescence intensity image of SK-BR3 cells incubated with AuNCs-Her (left) and AuNCs alone for 4 h (right). (B) Confocal images of breast cancer tissue (left) and normal breast tissue (right) as control incubated with AuNCs-Her. (C) FLIM of SK-BR3 cells stained by Lamin A antibody labeled with Alexa350, indicating nuclear uptake of AuNCs-Her (left) and AuNCs alone (right) incubated for 4 h as control. FLIM scale bar: 0 to 2 ns. (D) Endolysosomes of SK-BR3 cells incubated with AuNCs-Her for 4 h and stained by lysosensor marker blue. From left to right: Emission from Lysosensor (400−450 nm) and emission from AuNCs (650−720 nm).

conjugation of Herceptin to AuNCs. During synthesis, bovine serum albumin (BSA) that formed on the outer layer of AuNCs was carboxylated by glutaraldehyde and glycine, to which amino groups bearing Herceptin were functionalized through the EDC linkage.[33] TEM image further demonstrates that the as-prepared AuNCs-Her (Figure S1 in Supporting Information) clusters are distributed uniformly and no aggregates could be noted. The size of the AuNCs-Her was calculated to be ~3.5 nm after the conjugation of Herceptin, an increase of ~2.0 nm from the initial size of AuNCs. The chemical conjugation was further confirmed by monitoring the change in the diffusion time of naked clusters (0.46 ms) and clusters conjugated with Herceptin (0.73 ms) by fluorescence correlation spectroscopy (FCS). The increase in diffusion time observed could be attributed to an increase in the molecular weight of the gold clusters with and without Herceptin.

Cancer Cell and Tumor Tissue Targeting. SK-BR3 cells, a human breast cancer cell over-expressing HER2 on the cell membrane, were chosen as the target, and AuNCs-Her and AuNCs were incubated with the cells for 4 h. Figure 2 shows the confocal fluorescence images of the clusters in cells. The left side of panel D (Figure 2) shows emission from Lysosensor (400−450 nm), whereas the right shows emission from AuNCs (650−720 nm). Due to the specific interaction of Herceptin with ErbB-2 receptor, high uptake efficiency of the AuNCs-Her probes (Figure 2A, left) was noted as evident from the discrete bright spots, which was assumed to undergo an ErbB2 receptor-mediated endocytosis. Past reports have shown that nanoparticle endocytosis depends on the cell type, clathrin dependence, and the size or the shape of the nanoparticles.[34−36] Here, we found that the uptake of AuNCs without the antibody was rare compared to AuNCs-Her (Figure 2A, right) in ErbB-2 over-expressing SK-BR3 cells even after 4 h of incubation. To further confirm targeting specificity, AuNCs-Her probes were incubated with ErbB-2 under-expressing MDA-MB-468 cells as control. Control experiments show only an insignificant uptake, possibly due to nonspecific interaction (Figure S2, left). The targeting specificity of AuNCs-Her was further illustrated by comparing ErbB-2 receptor over-expressing breast cancer tumor tissues (infiltrating duct carcinoma) (Figure 2B, left) with normal tissues (Figure 2B, right). Almost no signal was observed from the normal tissues, while tumor tissues exhibited strong fluorescence due to targeting, further demonstrating that AuNCs-Her has strong specific binding with ErbB-2 receptors.

Endosome Escape for AuNCs-Her to the Nucleus. Interestingly, a strong bright spot was noted in Figure 2A (left), which was attributed to the accumulation of AuNCs specifically in the nucleus of cells. To further demonstrate the localization of the probes, Lamina A antibody was used as a nuclear envelop marker to specifically stain the inner nuclear membrane. Fluorescence lifetime imaging (FLIM) was used to separate the envelope and the inner regions based on their difference in lifetime as fitted by exponential decay fitting functions. Clear difference in the fluorescence lifetime of AuNCs (1.5 ns) and Lamina A antibody labeled with Alexa350 (1.9 ns) was noted (Figure 2C), indicating the presence of AuNCs in the nucleus. AuNCs were found to be distributed throughout the cytoplasm as well as in the chromosomal regions of the nucleus (Figure 2C, left). Compared to cells incubated with bare AuNCs, only the envelop marker could be visualized (Figure 2C, right). Our previous studies using gold nanorods (AuNRs) show that most of the Herceptin-conjugated AuNRs are entrapped in the endolysosomal system with minimal escape from the endosomes posing a major barrier for effective drug delivery and release.[37] Thus, nanomaterials capable of endosomal escape might have the ability to localize in the nucleus and could

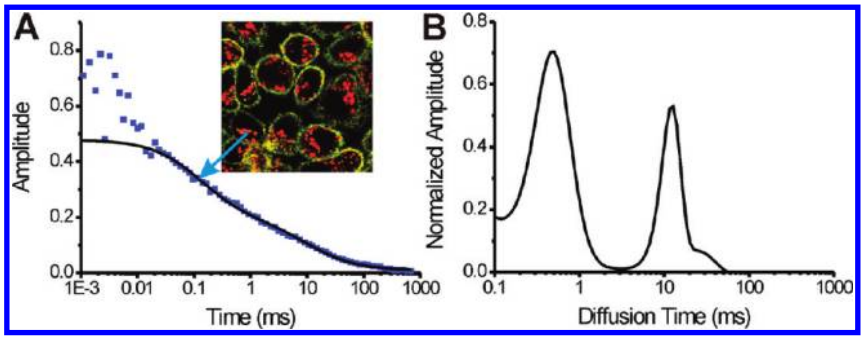

Figure 3. (A) Typical autocorrelation curve (solid squares) of AuNCs-Her diffusing inside the nucleus fitted with two components (black solid line). Inset is the image of SK-BR3 cells incubated with AuNCs-Her-Alexa647 for 4 h. (B) MEMFCS provides a measure of the diffusion time of AuNCs-Her-Alexa647.

serve as effective drug delivery and therapeutic agents. Experiments demonstrate that AuNCs are able to escape the endosome and enter the nucleus to impart therapy with high efficacy. Lysosensor was used to stain the endosomes and lysosomes of live SK-BR3 cells to monitor uptake of AuNCs-Her after 4 h of incubation. Confocal images show that a majority of AuNCs-Her did not accumulate within the endosome (Figure 2D), signifying their endosomal escaping ability. Super-resolution images obtained by structured illumination microscopy with 100 nm lateral resolution (ELYRA S.1, Carl Zeiss Inc.) showed part of AuNCs-Her localizing in the nucleus as indicated by discrete bright spots within the nuclear envelop and other AuNCs-Her localizing in the cytoplasm (Figure S3). As demonstrated through our endosome labeling experiments, AuNCs showed the capability of escaping from the endolysosomal system. This provides an opportunity for some of the AuNCs to freely diffuse through the nuclear pore simply due to its ultrasmall size. This process is unlikely to be mediated by specific transport protein since the AuNCs are not conjugated with nuclear localization sequence bearing peptides.

Dynamic Tracking of AuNCs-Her in the Nucleus of the Cells. Transport of proteins into the nucleus is an essential and important process in eukaryotic cells influencing gene regulation. Having demonstrated that AuNCs-Her could enter the nucleus, we attempt to determine the dynamics of these nanoscale probes in the nucleus of live cells using FCS. Herceptin-labeled with Alexa647 was first incubated with SK-BR3 cells for 4 h (control), and its localization in cells was tracked by confocal microscopy (the labeling of Alexa647 on Herceptin and AuNCs was confirmed by monitoring the diffusion time using FCS and fluorescence spectra, as shown in Figure S4). It was found that Herceptin primarily localized on the cell membranes and in specific intracellular compartments as expected. In addition, free Herceptin had very limited ability to pass through the nuclear pore complex.[38] However, single point FCS measurements confirmed the presence of AuNCs-Her in the nucleus of live SK-BR3 cells (Figure 3A) by monitoring the diffusion time and concentration from the autocorrelation plot. The autocorrelation curves of AuNCs-Her diffusion in the nucleus could be well fitted with a single component since a two-component free diffusion model did not improve the quality of fit of the autocorrelation functions of AuNCs diffusing in the nucleus (Figure 3A). The inset in Figure 3A shows the FLIM of live SK-BR3 cells after 4 h of incubation with AuNCs-Her. The yellow color represents the staining of the cell membrane. It is well-known that ErbB2 is predominantly expressed on the cell surface. Due to the specific interaction between Herceptin and ErbB2, it is clear that particles are internalized while some could possibly reside on the cell membrane even after 4 h of incubation. Maxima entropy method FCS (MEMFCS) was used to assess the diffusion of different species. MEMFCS is particularly suitable for the analysis of systems with heterogeneous diffusion time and does not need *a priori* to be assigned for fitting the diffusion time.[39] The diffusion time of AuNCs-Her in the cytoplasm was found to be ~0.8 ms (data not shown). Interestingly, we found that the diffusion of AuNCs-Her in the nucleus has two distinct peaks: one at ~0.5 ms and the other ~10 ms (Figure 3B). The faster diffusers could be attributed to the diffusion of AuNCs-Her in the nucleus with minor obstacles. The slower diffusers are possibly due to the interaction of the nanoclusters with nuclear proteins or chromatin structures or the complexity of traversing the nuclear matrix. The exact mechanism of the interaction between AuNCs and nuclear protein and its trajectory could be the subject for future explorations. The formation of larger aggregates in the nucleus is unlikely since no significant intermittent spikes could be found in the fluorescence fluctuation data. In addition to the diffusion dynamics, the absolute concentration of AuNCs-Her in the nucleus of live cells was also estimated by FCS. From the amplitude of the autocorrelation function, the concentration of AuNCs-Her in the nucleus was estimated to be 5−10 nM. This concentration was found to be sufficient to induce DNA damage and apoptosis.

DNA Damage and Apoptosis of AuNCs-Her to the Cells. Here we show that AuNCs-Her could escape the endosome/lysosome pathway and penetrate the nuclear pore

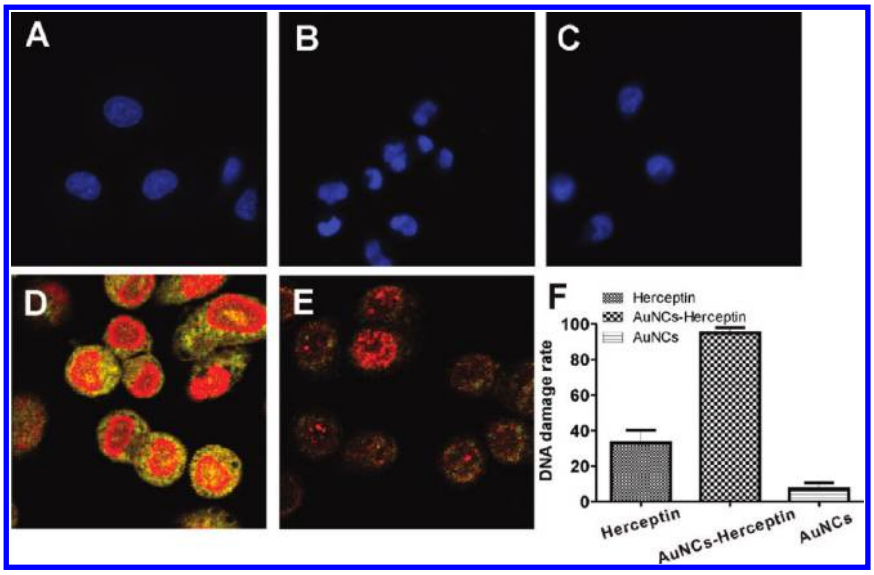

Figure 4. Fluorescence images show the apoptosis induced by AuNCs alone (A), AuNCs-Her (B), and Herceptin (C) by staining the nucleus with Hoechst 33258 (excited by UV light and the emission is 460 nm). Fluorescence lifetime imaging (FLIM) shows DNA damage of SK-BR3 cells induced by AuNCs-Her (D) and Herceptin alone (E) indicated by the bright yellow dots. Quantitative evaluation of DNA damage of cells as a percentage of the total number of cells for different treatments (F).

complex to enhance the therapeutic efficacy. Experiments indicate that AuNCs-Her has the potential to induce enhanced DNA damage and apoptosis in SK-BR3 cells because of its nuclear targeting ability. Hoechst 33258 binds preferentially to the A-T base pairs from the side of the minor groove of the DNA and can be used to visualize the apoptotic body formation and nuclear changes which are characteristic of apoptosis. Our results show that both Herceptin and AuNCs-Her could induce apoptosis while apoptosis could not be observed in cells treated with bare AuNCs (Figure 4A). Early DNA damage was signified by the phosphorylation of γ-H2A.X using appropriate anti-γ-H2A.X targeting antibodies. To further confirm our findings, cells were probed using the phosphorylated form of H2A.X (γ-H2A.X) antibody which signals the initial response to double-stranded break (DSB).[40−42] FLIM indicated that almost all of the cells cultured with AuNCs-Her had specific fluorescence staining, representing DNA damage (Figure 4D). In contrast, only a small amount of cells treated with Herceptin alone shows DNA damage under the same condition to indicate that the antitumor effect of AuNCs-Her is much higher than the treatment with Herceptin alone (Figure 4E). Quantification of apoptosis positive cells as a percentage of the total number of cells revealed that only 35% of the cells treated with Herceptin underwent apoptosis due to DNA damage compared to 95% of the AuNCs-Her (Figure 4F) treated cells ($p < 0.05$, $n = 500$). Cell death experiments (MTT assay) shown in Figure S5 further confirm that the antitumor activity of Herceptin could be enhanced by AuNCs due to nuclear targeting of AuNCs.

CONCLUSION

Collectively, our results demonstrate that fluorescent metal nanoclusters (AuNCs) conjugated with a targeting ligand (*e.g.*, Herceptin in our model) possess high targeting specificity and nuclear localization capability. These fluorescing probes can be used for simultaneous imaging and enhanced cancer therapy because of its ability to induce nuclear damage. Importantly, we found that the endocytosed AuNCs-Her could escape the endolysosomal pathway and has the ability to penetrate the nucleus possibly due to its small size effect. By employing FCS, the diffusion characteristics and concentration of AuNCs-Her in the nucleus was also elucidated. Our experiments further indicated that the therapeutic effect of Herceptin could be significantly enhanced possibly due to the nuclear targeting ability of AuNCs-Her and its endolysosomal escape, opening a new route to nuclear nanomedicine.

MATERIALS AND METHODS

Chemical Reagents. Hydrogen tetrachloroaurate (III) trihydrate ($HAuCl_4 \cdot 3H_2O$, 99%), BSA, glutaraldehyde, glycine, sodium borohydride, and *N*-(3-(dimethylamino)-propyl)-*N*′-ethylcarbodiimide (EDC) were obtained from Sigma-Aldrich Chemical Co. and used without further purification. All of the water used was purified with Milli-Q plus system (Millipore Co.), and the resistivity was kept to over 18 MΩ·cm.

Synthesis of Gold Nanoclusters. Gold nanoclusters (AuNCs) were synthesized according to the method proposed by Xie *et al.*[16] Briefly, 5 mL of 10 mM aqueous chloroauric acid solution (37 °C) was added to 5 mL of 50 mg/mL BSA solution (37 °C) under vigorous stirring. Two minutes later, 0.5 mL of 1 M NaOH

solution was introduced, and the mixture was incubated at 37 °C for 12 h. The color of the solution changed from light yellow to light brown and then to deep brown. Excess salt was removed through dialysis.

Characterization and Functionalization of AuNCs by Herceptin. As-prepared AuNCs were characterized by UV−vis absorption spectroscopy using a Jasco V570 UV/visible/NIR spectrophotometer (Jasco, Inc., Easton, MD) in the 200−900 nm wavelength range. Fluorescent emission spectra were obtained using the Cary fluorescent spectrometer.

The functionalization of AuNCs with Herceptin was carried out according to the method reported by Sun *et al.*[33] Glutaraldehyde was first introduced along with the AuNCs to form the cross-linked organic layer around AuNCs. The extra aldehyde functional groups on the AuNCs' surface were removed by treatment with glycine or sodium borohydride. Since most of the surface amino groups on the BSA are removed in this process, AuNCs carried a net negative charge from the carboxylic acid groups. The activation of carboxylic acid groups on the BSA molecule was achieved by treatment with EDC. Excess EDC was removed by centrifugation using the cutoff tube, and the resulting *O*-acylisourea intermediates are reacted with amino groups from Herceptin to form amide bonds between the encapsulation layer and Herceptin.

Since excess chemicals will be removed by centrifugation using the cutoff tube, contribution from the chemicals to the cell death is assumed to be negligible.

Cell Culture. SK-BR3 cells and MDA-MB-468 were maintained in RPMI medium 1640 (Sigma-Aldrich) supplemented with 10% fetal bovine serum (Sigma-Aldrich) and 1% penicillin/streptomycin (Sigma-Aldrich). Cultures were maintained at 37 °C and 5% CO_2 atmosphere. For living-cell fluorescence microscopy studies, cells were seeded onto sterilized No. 1 coverslip (VWR International, Batavia, IL) and placed inside a 12-well plate. After the cells reached 80% confluence, they were incubated with AuNCs, Herceptin, or AuNCs-Her at 37 °C and washed with minimum essential medium (MEM) three times. The culture was kept active, and the cells were taken out from the incubator for measurements at different time points (4 and 16 h) when needed.

Tissue Treatment. Breast tumor tissues and the normal tissues were treated according to the following protocol.

(a) Deparaffinization and hydration. Incubate the tissue in a dry oven at 60 °C for 1 h, dewax slides in freshly prepared xylene for 4 min five times, and slides were then hydrated in 100, 95, and 75% ethanol for 3 min twice. The slides were then immersed in tap water for 5 min.

(b) Antigen retrieval: 200−300 mL of H_2O was added in a rice cooker and allowed to boil for *ca.* 10 min. Next, the slides were placed inside the bottle filled with antigen retrievel buffer, incubated for 20 min, then rinsed in cold tap water for 3−5 min.

(c) Immerse slide in H_2O_2 for 6 min to reduce autofluoresence.

(d) Wash the slides in 0.025% Triton X-100 PBS for 3 × 5 min.

(e) Incubate the slides with blocking serum for 30 min to blot excess serum from section. Incubate the slides with AuNCs-Her at 4 °C overnight. Wash the slide in PBS for 3 × 10 min after which the samples are ready for imaging.

Endosomal Escape. To more clearly reveal the mechanism of AuNCs transfecting the nucleus of the cells, endosomal escape study was carried out. After the incubation of AuNCs-Her with cells for 4 h, cells were stained with endosome escape marker (Lysosensor) for 30 min. After washing with PBS three times, the cells were imaged by confocal fluorescence microscopy.

Nuclear Envelope. After incubation of the AuNCs, AuNCs-Her with SK-BR3 cells, cells on coverslips were fixed in 4% paraformaldehyde for 30 min, washed in PBS for 3 × 10 min, permeabilized for 10 min in 0.25% Triton X-100, and blocked in PBST with 1% BSA for 30 min at room temperature. The coverslips were incubated with the nuclear envelope marker (Lamin A antibody; Abcam, ab2559) for 1 h at room temperature or 4 °C overnight, washed in PBS for 3 × 10 min, and incubated with Alexa350-conjugated goat anti-rabbit secondary antibody (Invitrogen) for 1 h at room temperature. Cells were then washed in PBS for 3 × 10 min and then imaged by multiphoton microscopy.

DNA Damage and Apoptosis. DNA double-strand breaks (DSBs) in cancer cells incubated with AuNCs were verified using a fluorescently labeled antibody specific for the phosphorylated form of H2AX (γ-H2AX). Discrete nuclear foci can be visualized at the sites of DSBs. After the incubation of SK-BR3 cells with AuNCs, Herceptin, and AuNCs-Her, cells on coverslips were fixed in 4% paraformaldehyde for 30 min, washed in PBS for 3 × 10 min, permeabilized for 10 min in 0.25% Triton X-100, and blocked in PBST with 1% BSA for 30 min at room temperature. The coverslips were incubated with anti-γ-H2A.X antibody (Bethyl Laboratories, Inc.) for 1 h at room temperature or 4 °C overnight, washed in PBS for 3 × 10 min, and incubated with Alexa350-conjugated goat anti-rabbit secondary antibody (Bethyl Laboratories, Inc.) for 1 h at room temperature. The cells were then washed in PBS for 3 × 10 min and then imaged by multiphoton microscopy.

After incubation of SK-BR3 cells with AuNCs, Herceptin, or AuNCs-Her, the cells were fixed and stained by Hoechst 33258 dye to test for apoptosis.

MTT Assay. SK-BR 3 cells were seeded in a 96-well plate at a density of 10^4 cells per well in a 100 μL volume. Cells were further maintained at 37 °C for 24 h after treatment with AuNCs, Herceptin, or AuNCs-Her. Cell viability was then determined using an MTT (3-(4,5-dimethylthiazol-2-yl)-2,5-diphenyltetrazolium bromide) assay (MTT cell growth assay kit, Chemicon, USA). The AuNC-treated cells were incubated with the MTT reagent for 4 h (viable cells are capable of metabolizing the MTT reagent, while dead cells are not), and 100 μL of DMSO was added to each well and incubated for 30 min, and the absorbance at 570 nm was read. Each concentration was repeated in triplicate, and the results are expressed as percentages.

Antibody Labeling. Herceptin was labeled with AlexaFluor647 monoclonal antibody labeling kit (Invitrogen) according to manufacturer's instructions. Free fluorophores were removed using a spin filter (MWCO 10 kDa, KPL). Fluorescence correlation spectroscopy (FCS) was performed to confirm antibody labeling based on the difference in diffusion time between free fluorophores and labeled antibody as shown in Figure S4.

Fluorescence Lifetime Imaging. Fluorescence lifetime images were acquired using the Microtime 200 system (Picoquant Gmbh, Germany) fitted with picosecond lasers. Further details of the instrumentation can be found elsewhere.[37]

The fluorescence lifetime was obtained by fitting the TCSPC histograms with the multiexponential model.

$$I(t) = \sum_{i=1}^{n} \alpha_i \exp\left(-\frac{t}{\tau_i}\right) \quad (1)$$

where τ_i denotes the lifetime with amplitudes α_i. The values of τ_i and α_i were obtained through nonlinear least-squares fitting using the SymphoTime software (PicoQuant).

FCS and MEMFCS. The autocorrelation curve of fluorophore diffusing in solution was fitted to a 3D diffusion model using one or two components with the SymphoTime software (PicoQuant GmbH Berlin, Germany) and Origin Lab using the equation

$$G(\tau) = \sum \frac{1}{N_i}\left(1+\frac{\tau}{\tau_{D_i}}\right)^{-1}\left(1+\frac{\tau}{\tau_{D_i}\kappa^2}\right)^{-1/2} \quad (2)$$

where Ni and τ_{D_i} denote the number of fluorescent molecules in the detection volume and diffusion time of component *i*, respectively. The parameter κ and the lateral diffusion coefficient *D* can be obtained from

$$k = \frac{z_0}{w_0},\ D = \frac{w_0^2}{4\tau_D} \quad (3)$$

Here, κ is defined as the ratio of the axial beam size z and radius ω of the laser, and τ_D denotes the diffusion time of the fluorophore.

MEMFCS (maximum entropy method analysis of fluorescence correlation spectroscopy data) (2) was employed to

validate the autocorrelation function of AuNCs-Her-Alexa647 in the nucleus.

$$G(\tau) = \int \alpha_i \left(1+\frac{\tau}{\tau_D}\right)^{-1} \left(1+\kappa^2\frac{\tau}{\tau_D}\right)^{-1/2} d\tau_D \qquad (4)$$

S is defined as $S = \Sigma_i p_i \ln(p_i)$, where $p_i = \alpha_i/\Sigma\alpha_i$.

Acknowledgment. Partial funding from the Purdue Center for Cancer Research, the CTSI (Purdue-IUPUI), the NSF Grant No. 0945771, and the Bilsland Fellowship for J.C. is acknowledged. Professors Maiti and Periaswamy (TIFR, Mumbai) are acknowledged for providing the MEMFCS software. Herceptin was a generous gift from Genentech Inc. (San Francisco, CA). The authors thank the super resolution imaging group from Zeiss Inc. for their help in super-resolution imaging. Discussions with Dr. M. Rao from CCMB through the IUSSTF grant is appreciated.

Supporting Information Available: Figure S1 gives the TEM images of AuNCs-Her conjugate. Figure S2 shows the confocal fluorescence intensity of MDA-MB-468 cells and SK-BR3 cells with AuNRs-Her incubation. Figure S3 shows the super-resolution structured illumination microscopy image of AuNCs-Her in the nucleus of SK-BR3 cells. Figure S4 gives the autocorrelation functions of Herceptin labeled with Alexa647 and AuNCs conjugated with Herceptin-Alexa647 and absorption and fluorescent spectra of AuNCs-Her-647. Figure S5 compares the toxicity of AuNCs-Her, Herceptin alone, and AuNCs alone by MTT assay. This material is available free of charge *via* the Internet at http://pubs.acs.org.

REFERENCES AND NOTES

1. Al-Jamal, W. T.; Kostarelos, K. Liposome−Nanoparticle Hybrids for Multimodal Diagnostic and Therapeutic Applications. *Nanomedicine* **2007**, *2*, 85–98.
2. Rhim, W. K.; Kim, J. S.; Nam., J. M. Lipid−Gold-Nanoparticle Hybrid-Based Gene Delivery. *Small* **2008**, *4*, 1651–1655.
3. Zhang, Y.; Shang, M. Self-Assembled Coatings on Individual Monodisperse Magnetite Nanoparticles for Efficient Intracellular Uptake. *Biomed. Microdevices* **2004**, *6*, 33–40.
4. Sharma, A.; Tandon, A.; Tovey, J. C.; Gupta, R., Robertson, J. D.; Fortune, J. A.; Klibanov, A. M.; Cowden, J. W.; Rieger, F. G.; Mohan, R. R. Polyethylenimine-Conjugated Gold Nanoparticles: Gene Transfer Potential and Low Toxicity in the Cornea. *Nanomedicine*. **2011**, DOI: 10.1016/j.nano.2011.01.006.
5. Duncan, R. The Dawning Rra of Polymer Therapeutics. *Nat. Rev. Drug Discovery* **2003**, *2*, 347–360.
6. Gilles, E. M.; Frechet, J. M. J. Designing Macromolecules for Therapeutic Applications: Polyester Dendrimer Poly(ethylene oxide) "Bow-Tie" Hybrids with Tunable Molecular Weight and Architecture. *J. Am. Chem. Soc.* **2002**, *124*, 14137–14146.
7. Canine, B. F.; Wang, Y.; Ouyang, W.; Hatefi, A. Development of Targeted Recombinant Polymers That Can Deliver siRNA to the Cytoplasm and Plasmid DNA to the Cell Nucleus. *J. Controlled Release* **2011**, *151*, 95–101.
8. Messerschmidt, S. K. E.; Musyanovych, A.; Altvater, M.; Scheurich, P.; Pfizenmaier, K.; Landfester, K.; Kontermann, R. E. Targeted Lipid-Coated Nanoparticles: Delivery of Tumor Necrosis Factor-Functionalized Particles to Tumor Cells. *J. Controlled Release* **2009**, *137*, 69–77.
9. Farokhzad, O. C.; Langer, R. Impact of Nanotechnology on Drug Delivery. *ACS Nano* **2009**, *3*, 16–20.
10. Walther, C.; Meyer, K.; Rennert, R.; Neundorf, I. Quantum Dot−Carrier Peptide Conjugates Suitable for Imaging and Delivery Applications. *Bioconjugate Chem.* **2008**, *19*, 2346–2356.
11. Talcott, B.; Moore, M. S. Getting Across the Nuclear Pore Complex. *Trends Cell Biol* **1999**, *9*, 312–318.
12. Palakurthi, S. Yellepeddi, V. K.; Kumar, A. Nanocarriers for Cytosolic Drug and Gene Delivery in Cancer Therapy. In *Biomedical Engineering, Trends, Research and Technologies*; Komorowska, M. A., Olsztynska-Janus, S., Eds.; InTech: Rijecka, Croatia, 2011; Chapter 11, ISBN: 978-953-307-514-3.Poon, I. K.; Jans, D. A. *Tra*□*c* **2005**, *6*, 173–186.
13. Kang, B.; Mackey, M. A.; El-Sayed, M. A. Nuclear Targeting of Gold Nanoparticles in Cancer Cells Induces DNA Damage, Causing Cytokinesis Arrest and Apoptosis. *J. Am. Chem. Soc.* **2010**, *132*, 1517–1519.
14. Ghaderi, S.; Ramesh, B.; Seifalian, A. M. Fluorescence Nanoparticles "Quantum Dots" as Drug Delivery System and Their Toxicity: A Review. *J. Drug Targeting* **2010**, *19*, 475–86.
15. Wu, X.; Ming, T.; Wang, X.; Wang, P.; Wang, J.; Chen, J. High-Photoluminescence-Yield Gold Nanocubes: For Cell Imaging and Photothermal Therapy. *ACS Nano* **2010**, *4*, 113–120.
16. Xie, J.; Zheng, Y.; Ying, J. Y. Protein-Directed Synthesis of Highly Fluorescent Gold Nanoclusters. *J. Am. Chem. Soc.* **2009**, *131*, 888–889.
17. Bruchez, M.; Moronne, M.; Gin, P.; Weiss, S.; Alivisatos, A. P. Semiconductor Nanocrystals as Fluorescent Biological Labels. *Science* **1998**, *281*, 2013–2016.
18. Lin, C. A. J.; Lee, C. H.; Hsieh, J. T.; Yu, W. C.; Yang, H. Z.; Li, J. K.; Sperling, R.; Wang, H. H.; Chan, W. H.; Yeh, H. I.; *et al.* Synthesis and Surface Modification of Highly Fluorescent Gold Nanoclusters and Their Exploitation for Cellular Labeling. *Proc. SPIE* **2010**, *7575*, 757506.
19. Wu, X.; He, X. X.; Wang, K. M.; Xie, C.; Zhou, B.; Qing, Z. H. Ultrasmall Near-Infrared Gold Nanoclusters for Tumor Fluorescence Imaging *in Vivo*. *Nanoscale* **2010**, *2*, 2244–2249.
20. Retnakumari, A.; Setua, S.; Menon, D.; Ravindran, P.; Muhammed, H.; Pradeep, T.; Nair, S.; Koyakutty, M. Molecular-Receptor-Specific, Non-toxic, Near-Infrared-Emitting Au Cluster-Protein Nanoconjugates for Targeted Cancer Imaging. *Nanotechnology* **2010**, *21*, 055103.
21. Slamon, D. J.; Leyland-Jones, B.; Shak, S.; Fuchs, H.; Paton, V.; Bajamonde, A.; Fleming, T.; Eiermann, W.; Wolter, J.; Pegram, M.; *et al.* Use of Chemotherapy Plus a Monoclonal Antibody against HER2 for Metastatic Breast Cancer That Overexpresses HER2. *N. Engl. J. Med.* **2001**, *344*, 783–792.
22. Vogel, C. L.; Cobleigh, M. A.; Tripathy, D.; Gutheil, J. C.; Harris, L. N.; Fehrenbacher, L.; Slamon, D. J.; Murphy, M.; Novotny, W. F.; Burchmore, M.; *et al.* Efficacy and Safety of Trastuzumab as a Single Agent in First-Line Treatment of HER2-Overexpressing Metastatic Breast Cancer. *J. Clin. Oncol.* **2002**, *20*, 719–726.
23. Taatjes, D. J.; Koch, T. H. Nuclear Targeting and Retention of Anthracycline Antitumor Drugs in Sensitive and Resistant Tumor Cells. *Curr. Med. Chem.* **2001**, *8*, 15–29.
24. Wagstaff, K. M.; Jans, D. A. Nuclear Drug Delivery To Target Tumor Cells. *Eur. J. Pharmacol.* **2009**, *625*, 174–80.
25. Mayfield, S.; Vaughn, J. P.; Kute, T. E. DNA Strand Breaks and Cell Cycle Perturbation in Herceptin Treated Breast Cancer Cell Lines. *Breast Cancer Res. Treat.* **2001**, *70*, 123–129.
26. Costantini, D. L.; Villani, D. F.; Vallis, K. A.; Reilly, R. M. Methotrexate, Paclitaxel, and Doxorubicin Radiosensitize HER2-Amplified Human Breast Cancer Cells to the Auger Electron-Emitting Radiotherapeutic Agent (111) In-NLS-Trastuzumab. *J. Nucl. Med.* **2010**, *51*, 477–483.
27. Maiti, S.; Haupts, U.; Webb, W. W. Fluorescence Correlation Spectroscopy: Diagnostics for Sparse Molecules. *Proc. Natl. Acad. Sci. U.S.A.* **1997**, *94*, 11753–11757.
28. Bastiaens, P. I.; Squire, A. Fluorescence Lifetime Imaging Microscopy: Spatial Resolution of Biochemical Processes in the Cell. *Trends Cell. Biol.* **1999**, *9*, 48–52.
29. Alvisi, G.; Jans, D. A.; Guo, J.; Pinna, L. A.; Ripalti, A. A Protein Kinase CK2 Site Flanking the Nuclear Targeting Signal Enhances Nuclear Transport of Human Cytomegalovirus ppUL44. *Tra*□*c* **2005**, *6*, 1002–1013.
30. Wang, C. G.; Chen, J. J.; Talavange, T.; Irudayaraj, J. Gold Nanorod/Fe_3O_4 Nanoparticle "Nano-Pearl-Necklaces" for Simultaneous Targeting, Dual-Mode Imaging, and Photothermal Ablation of Cancer Cells. *Angew. Chem., Int. Ed.* **2009**, *48*, 2759–2763.
31. Rubart, M. Two-Photon Microscopy of Cells and Tissues. *Circ. Res.* **2004**, *95*, 1154–1166.
32. Lin, C. A. J.; Yang, T. Y.; Lee, C. H.; Huang, S. H.; Sperling, R. A.; Zanella, M.; Li, J. K.; Shen, J. L.; Wang, H. H.; Yeh, H. I.; *et al.*

Synthesis, Characterization, and Bioconjugation of Fluorescent Gold Nanoclusters toward Biological Labeling Applications. *ACS Nano* **2009**, *3*, 395–401.
33. Sun, L.; Sung, K. B.; Dentinger, C.; Lutz, B.; Nguyen, L.; Zhang, J.; Qin, H.; Yamakawa, M.; Cao, M.; Lu, Y.; *et al.* Composite Organic−Inorganic Nanoparticles as Raman Labels for Tissue Analysis. *Nano Lett.* **2007**, *7*, 351–356.
34. Chithrani, B. D.; Ghazani, A. A.; Chan, W. C. Determining the Size and Shape Dependence of Gold Nanoparticle Uptake into Mammalian Cells. *Nano Lett.* **2006**, *6*, 662–668.
35. Chithrani, B. D.; Chan, W. C. Elucidating the Mechanism of Cellular Uptake and Removal of Protein-Coated Gold Nanoparticles of Different Sizes and Shapes. *Nano Lett.* **2007**, *7*, 1542–1550.
36. Jiang, W.; Kim, B. Y.; Rutka, J. T.; Chan, W. C. Nanoparticle-Mediated Cellular Response is Size-Dependent. *Nat. Nanotechnol.* **2008**, *3*, 145–150.
37. Chen, J.; Irudayaraj, J. Quantitative Investigation of Compartmentalized Dynamics of ErbB2 Targeting Gold Nanorods in Live Cells by Single Molecule Spectroscopy. *ACS Nano* **2010**, *3*, 4071–4079.
38. Costantini, D. L.; Chan, C.; Cai, Z; Vallis, K. A.; Reilly, R. M. (111)In-Labeled Trastuzumab (Herceptin) Modified with Nuclear Localization Sequences (NLS): An Auger Electron-Emitting Radiotherapeutic Agent for HER2/neu-Amplified Breast Cancer. *J. Nucl. Med.* **2007**, *48*, 1357–1368.
39. Sengupta, P.; Garai, K; Balaji, J.; Periasamy, N.; Maiti, S. Measuring Size Distribution in Highly Heterogeneous Systems with Fluorescence Correlation Spectroscopy. *Biophys. J.* **2003**, *4*, 1977–1984.
40. Chen, H. T.; Bhandoola, A.; Difilippantonio, M. J.; Zhu, J.; Brown, M. J.; Tai, X. G.; Rogakou, E. P.; Brotz, T. M.; Bonner, W. M.; Ried, T.; *et al.* Response to RAG-Mediated V(D)J Cleavage by NBS1 and γH2AX. *Science* **2000**, *290*, 1962–1964.
41. Petersen, S.; Casellas, R.; Reina-San-Martin, B.; Chen, H. T.; Difilippantonio, M. J.; Wilson, P. C.; Hanitsch, L.; Celeste, A.; Muramatsu, M.; Pilch, D. R.; *et al.* AID is Required To Initiate Nbs1/γ-H2AX Focus Formation and Mutations at Sites of Class Switching. *Nature* **2001**, *414*, 660–665.
42. Schier, A. F.; Talbot, W. S. Molecular Genetics of Axis Formation in Zebrafish. *Annu. Rev. Genet.* **2005**, *39*, 561–613(Review).